Conf-930830--11-Rev.1

UCRL-JC-111969 Rev 1
PREPRINT

The Optical Constants and Spectral Specular Reflectivity of Highly Oriented Pyrolytic Graphite (HOPG)

Mark A. Havstad
Marcus A. Schildbach
William McLean II

This paper was prepared for submittal to the
1993 National Heat Transfer Conference
Atlanta, Georgia
August 8-11, 1993

August 1993

Abstract

Measurements of the specular reflectivity and the optical constants of highly ordered pyrolytic graphite (HOPG) have been made using two independent optical systems. The first measures reflectance (at 1.06 μm and 293 K) by comparing the intensity of a laser beam before and after reflecting off the sample. The second determines the complex index of refraction (from 0.55 to 8.45 μm, with sample temperatures of 293, 480, 900 and 1300 K) by ellipsometry. Agreement between the two methods is good. Moderate reflectivitities are observed over the full spectral range of measurement: the spectral directional-hemispherical reflectivity at normal incidence varies from 0.41 at 0.55 μm to 0.74 at 8.45 μm. The components of the complex index of refraction increase smoothly with wavelength. The index of refraction increases from 3.10 at 0.55 μm to 7.84 at 8.45 μm. The extinction coefficient varies from 2.01 to 6.66 over the same range. The results are of interest to studies of laser-material interaction, to the search for accurate and durable reflectance standards a: d to the study of the optical constants and thermal radiative properties of materials.

1. Introduction

The thermal radiative properties of the surfaces of materials are of importance to a wide range of research and development activities, for example, welding, casting, and the interaction of lasers with materials. Detailed modeling of such processes can now include radiative transport between surfaces with angular, spectral and specular effects considered. Accurate information is required on the three surface radiative properties (reflectance, emittance and absorptance) as a function of wavelength, temperature, and angle relative to the surface normal. Here, we report measurements of the specular reflectance and the optical constants of highly oriented pyrolytic graphite (HOPG).

HOPG is of interest as a standard material for surface reflectance. Its high as-produced flatness, very low reactivity, lack of grain boundaries and compatibility with high temperature in vacuum make it attractive for verifying the performance of the many experimental arrangements presently used to measure reflectance. HOPG can be a simple, inexpensive and stable reference material and can be used over a broad range of wavelengths and conditions. Presently, the reference reflectors available in the U.S. (from the NIST, formerly NBS) are useful only in narrow wavelength and temperature ranges.

Comparisons between the measured thermal radiative properties of HOPG and calculations based on the classical theories of the optical constants are also of interest. HOPG, like the transition metals, does not display free electron-like optical properties. The relative simplicity of both the carbon atom and its arrangement in HOPG may allow for the beginnings of a more effective model which eventually could be extended to transition metals such as tungsten and molybdenum.

In many prior studies of thermal radiative properties, insufficient attention has been paid to the surface condition. A review of the reported work leads to very low confidence in the results (because of the large scatter in the data) to the point where the results from various workers rarely

agree within their stated uncertainty limits. Estimates of contamination based on the reported system pressures often indicate a high probability of significant surface impurities. This problem is minimized with the basal plane of HOPG which, being inert, will not suffer from contamination that will cause the surface properties to vary over time or from sample to sample. Unlike most metallic surfaces, HOPG will also not vary significantly with preparation technique (such as polish, evaporation conditions, grain orientation or exposure history) so it can be periodically measured in reflectometers or other devices used for determining the thermal radiative properties to check for systematic errors and to determine instrument precision.

2. Theoretical Background

Relations for the reflectivity of surfaces as a function of angle of incidence, material properties and polarization follow from Maxwell's equations and the boundary conditions for continuity of electric and magnetic field across an interface [1]. For electromagnetic radiation incident on a planar interface between two materials, the amplitude reflection coefficients for the parallel and perpendicularly polarized (relative to the interface normal) components of the electric field vector are:

$$r_{\lambda,p} = \frac{E_p^r}{E_p} = \frac{\cos\theta / \cos\chi - (n_1 - ik_1)/(n_2 - ik_2)}{\cos\theta / \cos\chi + (n_1 - ik_1)/(n_2 - ik_2)}$$

$$r_{\lambda,s} = \frac{E_s^r}{E_s} = \frac{\cos\chi / \cos\theta - (n_1 - ik_1)/(n_2 - ik_2)}{\cos\chi / \cos\theta + (n_1 - ik_1)/(n_2 - ik_2)} \qquad (1)$$

Parallel polarization is denoted p and perpendicular polarization is denoted s (from the German word senkrecht for perpendicular). Upon reflection, each component of polarization undergoes a phase shift and an amplitude attenuation which depends on the angle of incidence and the complex indices of refraction of the two materials. The real part of the complex index is n, which relates to the bending of a ray as it crosses an interface. The imaginary part is the extinction coefficient, k,

which describes the attenuation of a wave as it propagates through a medium. The angle of refraction, χ, is related to the angle of incidence and the optical constants by Snell's law.

Thermal radiative properties are related to the square of the amplitude reflection coefficients, the intensity reflection coefficients, which are given by the Fresnel equations. These equations are commonly used in heat transfer because they give the fraction of incident energy reflected for each component of polarization. For a wave in vacuum incident on a planar surface of an isotropic material with complex index of refraction (n+ik):

$$\rho_{\lambda,p} \equiv r^2_{\lambda,p}(\lambda,\theta) = \frac{a^2 + b^2 - 2a\sin\theta\tan\theta + \sin^2\theta\tan^2\theta}{a^2 + b^2 + 2a\sin\theta\tan\theta + \sin^2\theta\tan^2\theta} r^2_{\lambda,s}$$

$$\rho_{\lambda,s} \equiv r^2_{\lambda,s}(\lambda,\theta) = \frac{a^2 + b^2 - 2a\cos\theta + \cos^2\theta}{a^2 + b^2 + 2a\cos\theta + \cos^2\theta}$$

$$\text{where } 2a^2 = \left[(n^2 - k^2 - \sin^2\theta)^2 + 4n^2k^2 \right]^{1/2} + (n^2 - k^2 - \sin^2\theta)$$

$$\text{and } 2b^2 = \left[(n^2 - k^2 - \sin^2\theta)^2 + 4n^2k^2 \right]^{1/2} - (n^2 - k^2 - \sin^2\theta) \qquad (2)$$

Since any polarized incident light can be represented by a linear combination of perpendicular and parallel polarized incident beams, the Fresnel equations give a complete description of surface reflectivity from smooth isotropic materials. The wavelength dependence indicated in the relations is a consequence of the dependence of n and k on wavelength. Because the complex index also depends on temperature, the polarized reflectivities depend on temperature, although this dependence is not indicated by the notation. The assumption of a planar reflection interface and an isotropic material leads to a dependence only on θ, (the polar angle) in the results for polarized reflectivity. Many real materials are not isotropic so that a full description of their properties involves the azimuthal angle also.

The ellipsometric method used here was developed simultaneously by Beattie and Conn [2,3] and Hodgson [4] in 1955. Because it does not employ the narrow band wave plates common

in many ellipsometers, this method is readily applied over the broad spectral regions of interest to heat transfer, although historically it has been used for studies of solid state physics [5-7].

With the method of Beattie and Conn, a beam of arbitrary polarization passes through a linear polarizer and reflects off the material of interest. This first linear polarizer, called the polarizer, is rotatable with rotation axis coincident with the beam axis. After reflection the beam passes through a second polarizer, referred to as the analyzer, which is rotatable about an axis coincident with the axis of the reflected beam. The linearly polarized beam becomes an elliptically polarized beam after reflection from the sample surface, and the intensity variation of the radiation transmitted by the analyzer can yield the salient parameters of the polarization ellipse of the reflected radiation [8].

The dependence of the intensity at the detector on the azimuthal positions of the polarizer and analyzer is :

$$\frac{I}{E^2 r_s^2} = \sin^2 \psi_N \sin^2 \psi_A + \rho\hat{}^2 \cos^2 \psi_N \cos^2 \psi_A + \frac{1}{2} \rho\hat{} \sin (2 \psi_N) \sin (2 \psi_A) \cos \Delta \qquad (3)$$

where Δ is the relative phase shift on reflection, $\rho\hat{}$ the amplitude ratio on reflection, ψ_A is the analyzer position, ψ_N is the polarizer position and E is the electric field vector.

With the polarizer fixed at 45° (relative to the plane of incidence) ψ is determined by the ratio of the intensities at two azimuths of the analyzer, namely zero and 90°. Thus, from (3) one obtains:

$$I_1 \equiv I (\psi_N = 45°, \psi_A = 90°) = I_o \sin^2 (45°) = \frac{I_o}{2} \qquad (4)$$

$$I_2 \equiv I(\psi_N=45^\circ,\psi_A=0^\circ) = I_o\,\rho\hat{}^2\cos^2 45^\circ = \frac{I_o}{2}\rho\hat{}^2 \qquad (5)$$

where $I_o = I(\psi_N=90^\circ,\psi_A=90^\circ)$

From the ratio of (4) and (5) one obtains:

$$\rho\hat{}(\theta) = \tan\psi = \sqrt{I_2 / I_1} \qquad (6)$$

Two more intensity readings are taken with the analyzer at ±45° (relative to the plane of incidence) with the polarizer position unchanged. These readings give:

$$I_3 \equiv I(\psi_N=45^\circ,\psi_A=45^\circ) = I_o\,(1+\rho\hat{}^2+2\rho\hat{}\cos\Delta)/4. \qquad (7)$$

$$I_4 \equiv I(\psi_N=45^\circ,\psi_A=-45^\circ) = I_o\,(1+\rho\hat{}^2-2\rho\hat{}\cos\Delta)/4. \qquad (8)$$

In principle either I_3 or I_4 can be used separately with I_1 and I_2 to obtain the phase shift Δ. However, when the reflectivity is high, as it is for metals at long wavelengths, Δ is then sensitive to small measurement errors. Using a combination of (7) and (8) reduces this sensitivity:

$$\cos\Delta = \left\{\frac{1}{2}\left(\rho\hat{} + \frac{1}{\rho\hat{}}\right)\right\}\left\{(I_3 - I_4)/(I_3 + I_4)\right\} \qquad (9)$$

The use of (9) still presents problems in the classical long wavelength limit for conductors, $\rho\hat{} \to 1$ and $\Delta \to 0$, where all methods become insensitive. However, the method of Beattie and Conn allows one to go to longer wavelengths than methods not using both phase shift and amplitude attenuation on reflection [9].

3. Experimental set up

A The ellipsometric system

Measurements were made while the sample was in an ultra-high vacuum chamber. Ultimate pressure, after bakeout was ~3. x 10^{-10} torr. The vacuum system (including an Auger spectrometer and two ion sputter guns) was described in earlier reports [10,11]. Auger spectra of the graphite revealed no contamination, even without sputtering.

The need for a spectrally broadbanded optical method with good sensitivity from the visible to 10 μm dictated that the measurement technique consider both phase shift and amplitude attenuation. The method of Beattie and Conn (or variants of it such as Miller's method [12]) was required. The technique of Beattie and Conn was selected and an original radiation source was developed [13] to cover an expanded wavelength range. The source consists of a hot element constructed of carbon composite board and maintained in a separate vacuum system.

A CaF_2 lens (Fig. 1) in front of the source forms an image of the hot element at an aperture ~150mm from the source exit window. This aperture rejects emission from the hot element's edges where non-random polarization was expected. An optical chopper placed just behind this aperture permits phase sensitive detection. Beyond the chopper is a second CaF_2 lens which collimates the chopped beam for passage through the polarizer.

Two types of polarizers were used. Calcite ($CaCO_3$) polarizers, which have an excellent extinction ratio (10^{-5} or better) were used from 0.4 to 2.3 μm. Beyond 2.3 μm calcite is absorbing so wire grid polarizers were used from 2.3 to 10 μm. Transmission losses and chromatic effects from the various CaF_2 elements prevented work beyond 10 μm. The polarizers were held and

rotated in a mount which allowed them to be centered in the incoming beam and aligned with their rotation axis coincident with the beam axis. Either type of polarizer could be positioned in these mounts and translated in the two directions perpendicular to the beam axis.

Following the polarizer, a focusing lens forms an image of the radiation source at the sample. Ellipsometric measurements have been made with the vacuum chamber at 760 torr and at 10^{-9} torr to establish that stress induced birefringence in the CaF_2 windows was insignificant. Since all the lenses were plano-concave their focal lengths varied over the spectral range of measurements. Images sharp in the visible at the sample or the detector were not as sharp in the infrared (at the same axial position). However, errors due to chromatic effects were small because in the ellipsometric measurement technique (described above) all data was obtained merely by rotating a single polarizer about the beam axis. Chromatic effects caused 1) a loss of signal due to vignetting at the apertures and 2) a variation in polarizer extinction ratio due to a variation in the beam collimation at both the polarizer and the analyzer.

Outside the vacuum chamber, another CaF_2 lens collimates the beam for passage through the second polarizer, the analyzer. A final focusing lens formed an image of the radiation source at an aperture directly in front of the detector. Band pass filters were placed directly in front of this last aperture. The detector consisted of an indium antimonide (InSb) photodiode backed by a mercury cadmium telluride (HgCdTe) strip operated as a photoconductor (a so called sandwich configuration). The front element of the sandwich is sensitive from 0.5 to 6 μm and transmits longer wavelengths. The HgCdTe photoconductor is sensitive from ~6 to 12 μm. When extra sensitivity in the visible was desired, a silicon photodiode was used from 0.4 to 1.1 μm.

B ¢ The reflectometer

The specular reflectivity at 1.06 μm was measured in 5° increments at room temperature in air on the basal plane of a freshly cleaved 1" by 1" sample attached to a rotatable mount. The position of the light source was fixed , requiring that the target be rotated and the detector moved.

The incident radiation was provided by a JK HY750 Nd:YAG laser operating without Q-switching to prevent surface modification [14]. The orientation of the polarization of the incident radiation relative to the graphite was controlled with a $\lambda/2$ plate and a thin film polarizer. The radiation intensity was measured by averaging 100 pulses with a Laser Precision RJP 735 pyroelectric probe. A positive lens was used to decrease the laser beam diameter at the sample surface.

4. Results

The two measurement techniques are compared in figures 2 and 3. The smooth curves were computed from the complex index of refraction obtained by the ellipsometer. The squares are the direct measurements of the reflectometer. Agreement between the two techniques is particularly good at the minimum in parallel polarized reflectivity, elsewhere differences between the two are usually less than 0.05 absolute units. An exception occurs at 85° (for the parallel component) where the reflectivity is changing very rapidly. The correlation coefficient, r, between the results for the two techniques are 0.914 for the parallel polarized component and 0.978 for the perpendicular component.

The normal spectral emissivity of HOPG is given in Fig. 4. The curves shown are least squares fits of the following form:

$$\varepsilon_n(\lambda) = a_c + \frac{i}{a_1\lambda^2 + a_2\lambda + a_3} \qquad (10)$$

This form is similar that derived by Edwards and DeVolo [15] from the work of Roberts [16] (which assumes contributions to the emissivity from both free and bound electrons). Coefficients for the fits are given in table 1. The variation of normal spectral emissivity with wavelength is qualitatively similar to that of many metals; a monotonic decrease with increasing wavelength from the visible to the infrared. However, lower values of emissivity (and higher values of reflectivity) are typical of metals, particularly beyond 3 to 5 μm.

The variation of emissivity with temperature is weak for visible wavelengths. Beyond about 4 μm the material exhibits lower emissivity and higher reflectivity as temperature increases because the extinction coefficient, k, increases with temperature and the index of refraction decreases with temperature ($\varepsilon_n = 4n/((n+1)^2 + k^2)$).

The variation of both of these components of the complex index of refraction (with wavelength and temperature) is given in figures 5 and 6. The values of k shown, between 2.01 at 0.55μm and 6.66 at 8.45 μm, indicate that, optically, this material more closely resembles a conductor than an insulator. However, at ambient temperature, the variation of n with wavelength is unlike a typical metal in that n is greater than k (over the full spectral range) and the magnitude of the increase in each component is far less than would be typical for even a transition metal such as tungsten or uranium. Highly conductive metals, such as copper, platinum and aluminum, display a yet greater increase in n and k between the visible and 10 μm (For aluminum at 10 μm, n is 25.3 and k is 89.8 [17]). Coefficients for the polynomial fits of figures 5 and 6 are given in table 2.

The optical constants of a material can be equivalently expressed in an alternate manner which is more conducive to comparison with theory. The complex dielectric function and the optical conductivity are simply related to the complex index of refraction:

$$\epsilon' = n^2 - k^2 \qquad (11)$$

$$\sigma = \epsilon''\omega\epsilon_o = 2nk\omega\epsilon_o \qquad (12)$$

where $\epsilon = \epsilon' + i\epsilon''$ and

ϵ_o is the permittivity of free space

Thus, the real part of the complex dielectric function, given in figure 7, and the optical conductivity, given in figure 8, present the same data as figures 5 and 6. Below 0.5 eV ($\lambda > 5$ μm), the scatter in the data is increased over what it was for n or k because of the squared

dependence in (11). The results for conductivity, the lossy component, are more strongly dependent on temperature. The local maximum at 0.95 eV (among the low temperature data) is of note (for ordinary graphite this peak has been reported at 0.8 eV [18]). As temperature increases the peak becomes less pronounced and shifts to lower energies. Aluminum displays the same trend as it is heated from ambient to liquid [19].

5. Discussion

Interpretation of the radiative properties and optical constants in terms of theories and other physical properties is desirable both for general understanding and for reducing the number of measurements needed to specify properties required for engineering analysis. Insight is often gained from the simple harmonic oscillator model (proposed by Lorentz) for the interaction of electromagnetic radiation and matter:

$$m\ddot{x} + D\dot{x} + Kx = eE \qquad (13)$$

The electron (with charge e and mass m) is bound to the ion core by the spring constant K. The damping constant for the oscillation is D and the driving force is due to the electric field of the incident radiation, E. In the limit of long wavelengths (low frequencies) and electrons not bound to the ion cores (K=0) one obtains the Hagen-Rubens relations. These were first derived by Drude and confirmed experimentally by Hagen and Rubens:

$$n = k = \sqrt{\frac{0.003\,\lambda_o}{r_e}} \qquad (14)$$

$$\varepsilon_n(\lambda_0) = 0.365\sqrt{\frac{r_e}{\lambda_o}} - 0.0464\,\frac{r_e}{\lambda_o} \qquad (15)$$

The direct current resistivity is r_e and the free space wavelength is λ_0. Although agreement with measurements is sometimes noted for wavelengths as low as 2 μm, it should not be expected until well beyond 10 μm. For some materials, agreement in the 2 to 10 μm range has been fortuitous

(due to surface imperfections such as roughness and oxidation). However, at longer wavelengths, n and k tend to increase rapidly, tend toward equality and the above two relations hold.

Inclusion of the inertial term (but not the restoring force) gives the free electron model: charges are free to move about between the ion cores of a material. The optical constants are then a function of two parameters, often taken to be the carrier density, N_e, and the collision time for electrons, τ:

$$\epsilon' = 1 - \frac{N_e e^2 \tau^2}{m\epsilon_o(1+\omega^2\tau^2)} \qquad (16)$$

$$\sigma = \epsilon'' \omega \epsilon_o = \frac{N_e e^2 \tau}{m(1+\omega^2\tau^2)} \qquad (17)$$

(The circular frequency of the incident radiation is ω.) This formulation works well for noble metals in the infrared and in some cases to near the visible. For molten aluminum it agrees well with data even into the visible. However, for most engineering materials it is inadequate, even at wavelengths as long as 10 μm.

The results given in figures 7 and 8 can not be well fit to the above relations with the assumption of constant carrier density and relaxation time because the electrons which interact with the incident radiation are not entirely unbound. One simple response to this failure of the free electron approach is to try to subsume bound effects into a variable carrier density. The quantum mechanical sum rule yields a carrier density, n_{eff}, as a function of photon energy, E. In terms of the results for conductivity:

$$n_{eff} = \frac{m}{2h\pi^2 N_a e^2} \int_0^{E_o} \sigma dE \qquad (18)$$

where N_a is the atomic density and

h is Planck's constant

The result of this integration (performed on curve fits to the data for each temperature) are shown in figure 9. The number of effective carriers is low and increasing over most or all of the range of measurement. These variable electron density functions were substituted in (16) above but again a good fit to the data was not obtained (this time the single assumption is that of a constant collision time for electrons). Thus, the bound electron effects in HOPG prevent use of the free electron relations.

The data might also be fit to an harmonic oscillator formulation in which free and multiple types of bound oscillators are posited to exist:

$$n^2 - k^2 - 2ink = 1 + \frac{N_a e^2}{\varepsilon_o m}\left[\frac{f_e}{\omega^2 + i\gamma_e\omega} + \sum_j \frac{f_j}{\omega_{oj}^2 - \omega^2 + i\gamma_j\omega}\right] \qquad (19)$$

where f_e is the is the number of unbound carriers per atom,

f_j is the number of bound oscillators of type j per atom,

γ_e and γ_j are damping constants and ω_{oj} is the resonant frequency of bound oscillator type j.

This approach is also unsatisfactory, because for most metals there is no long wavelength spectral range in which unbound electron effects occur to the exclusion of bound ones (for tungsten, one of the bound (or interband) effects is spin-orbit splitting and it occurs at photon energies as low as .33 to .40 eV [20j).

6. Conclusion

HOPG can provide a smooth stable surface for repeatable reflectivity measurements. The optical constants have been provided between 0.55 μm and 8.45 μm and they are similar to those of moderately conducting metals. When the optical constants are presented in terms of the complex dielectric function rather than the complex index of refraction, additional information is obtained,

including the effective number of free carriers per atom. However, even with a carrier density varying with photon energy, the data does not fit the free electrons relations.

This work was performed under the auspices of the U.S. Department of Energy by Lawrence Livermore National Laboratory under contract No. W-7405-Eng-48.

1. J.D. Jackson, Classical Electrodynamics, 2nd ed., John Wiley and Sons, New York (1975).
2. J. R. Beattie, "Optical Constants of Metals in the Infra-Red—Experimental Methods," Phil. Mag., **46**, 235 (1955).
3. J. R. Beattie and G. K. T. Conn, "Optical Constants of Metals in the Infra-Red—Principles of Measurement," Phil. Mag., **46**, 222 (1955).
4. J.N. Hodgson, "The Infrared Properties of Some Metallic Films," Proc. Phys. Soc., **9** (B), 593 (1955).
5. E.T. Arakawa, T. Inagaki and M.W. Williams, "Optical Properties of Metals by Spectroscopic Ellipsometry," Surface Science, **96**, 248 (1980).
6. H.G. Liljenvali, A.G. Mathewson and H.P. Myers, "The Optical Properties of Lead in the Energy Range 0.6–6 eV," Phil. Mag., **22**, 243 (1970).
7. A. Faldt and P.O. Nilsson, "Optical Properties of Thorium in the Range 0.5–25 eV," Physical Review B, **22**, 1740 (1980).
8. D. Clarke and J.F. Grainger, Polarized Light and Optical Measurement, Pergammon Press, Oxford (1971).
9. M.A.Havstad and S.A.Self, "Sensitivity Analyses of measurement methods for the optical constants of metals in the spectral range 0.4 to 10 μm,"International Journal of Thermophysics (submitted for review).
10. M. A. Havstad, W. McLean, S. A. Self, "Apparatus for the Measurement of the Optical Constants of Metals in the Spectral Range 0.4 to 10 μm,"Review of Scientific Instruments, (submitted for review).
11. M. A. Havstad, The Radiative Properties and Optical Constants of liquid Metals, UCRL-LR-107524, Lawrence Livermore National Laboratory, (1991).
12. J.C. Miller, "The Optical Properties of Liquid Metals at High Temperature," Phil. Mag., **20**, 1115 (1969).
13. M.A.Havstad,S.A.Self,D.L.Brown,J.D.Maltby and J.L.Ebert,"A simple radiation source for both the visible and the infrared,"Infrared Physics, (accepted for publication).
14. M.A. Schildbach, R.J.Tench, M. Balooch and W. J. Siekhaus, "Scanning tunneling microscope observations of pulsed laser modification of the basal plane of graphite," Materials Letters, **13**, 169 (1992).
15. D. K. Edwards and N. Bayard de Volo, "Useful Approximations for the Spectral and Total Emissivity of Smooth Bare Metals," Advances in Thermophysical Properties at Extreme Temperatures and Pressures, ASME, New York (1965).
16. S. Roberts, "Optical Properties of Nickel and Tungsten and Their Interpretation According to Drude's Formula," Physical Review, **114**, 104 (1955).
17. W.R. Hunter, "Measurement of Optical Constants in the Vacuum Ultraviolet Spectral Region," Chapter 4, Handbook of Optical Constants of Solids, E. D. Palik, Editor, Academic Press. New York (1985).
18. E.A. Taft and H.R. Philipp, "Optical Properties of Graphite," Physical Review,138,A197 (1965)
19. A. G. Mathewson and H. P. Myers, "Optical absorption in aluminum and the effect of

temperature,"J.Phys. F.: Metal Phys., **2**, 403 (1972).
20. L.V. Nomerovannaya, M.M. Kirillova and M.M.Noskov, "Optical properties of tungsten monocrystals," **33**, 405 (1971).

Nomenclature

a	term in the Fresnel equations
a_0,a_1,a_2,a_3	constants in fit of emissivity vs. wavelength
b	term in the Fresnel equations
D	damping constant
e	electronic charge
E	energy
E	electric field vector
f	number of oscillators per atom
i	imaginary numb r
I	intensity
I_o	reference intensity in ellipsometric technique
I_1,I_2,I_3,I_4	measured variables in ellipsometric technique
k	extinction coefficient
K	spring constant
m	mass
n	index of refraction
N	number density
r_e	direct current resistivity
r	amplitude reflection coefficient
T	temperature
x	displacement

GREEK

ε	emissivity
γ	damping term
θ	angle
λ	wavelength
ρ	intensity reflection coefficient
$\rho^{\wedge}$	the ratio of amplitude reflection coefficients
χ	angle of refraction
ψ	angle used in ellipsometry
ψ_A	azimuth of analyzer in ellipsometry
ψ_N	azimuth of polarizer in ellipsometry
τ	collision time for electrons

σ	conductivity
ω	angular frequency in radians per second
Δ	relative phase shift on reflection
ϵ'	real part of complex dielectric function
ϵ''	imaginary part of complex dielectric function
ϵ_0	permittivity of free space

SUBSCRIPTS

a	atomic
e	electronic
eff	effective
A	analyzer of ellipsometer
j	oscillator index
n	normal
N	polarizer of ellipsometer
o	free space value or resonant value
p	parallel component
r	reflected
s	perpendicular componenty
λ	wavelength

SUPERSCRIPTS

r	reflected

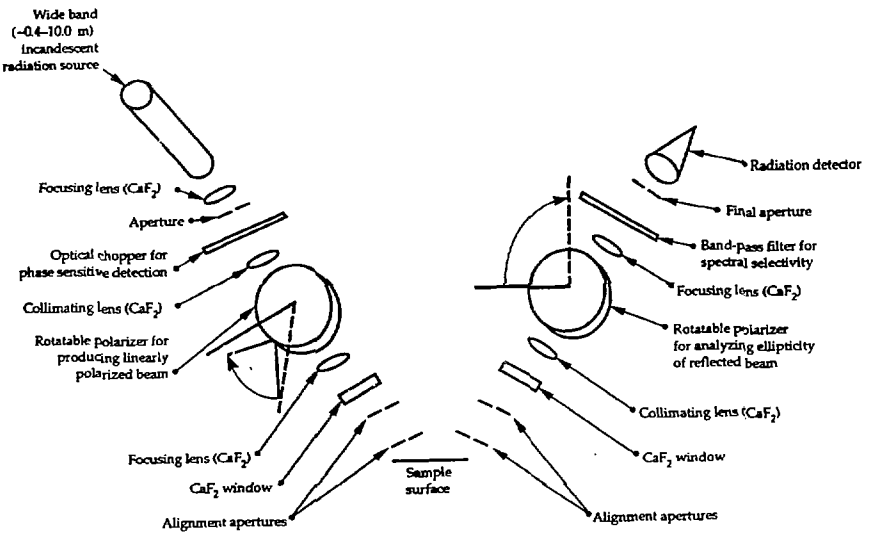

Fig. 1. Schematic of the ellipsometry measurement system.

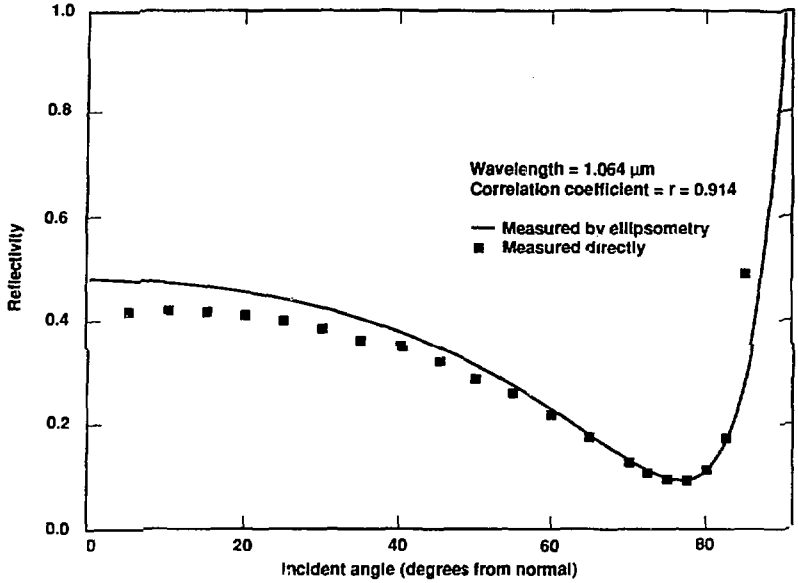

Fig. 2. A comparison of measurements of the parallel polarized reflectivity of Highly Ordered Pyrolytic Graphite (HOPG)

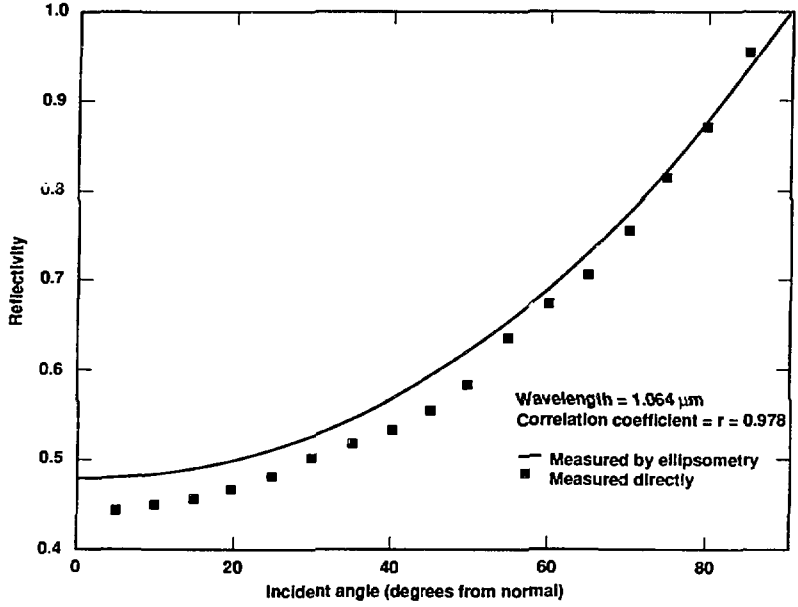

Fig. 3. A comparison of measurements of the perpendicularly polarized reflectivity of Highly Ordered Pyrolytic Graphite (HOPG)

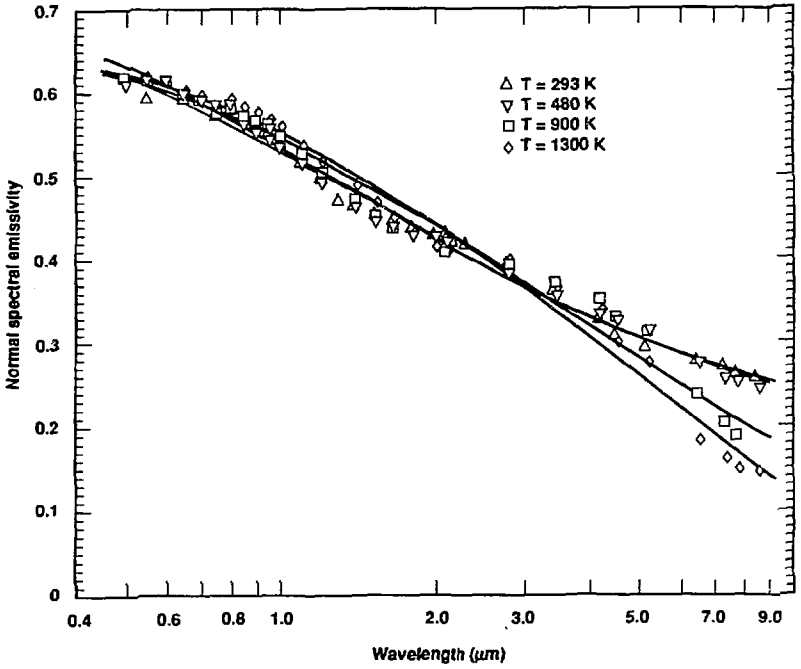

Fig. 4. The normal spectral emissivity of HOPG.

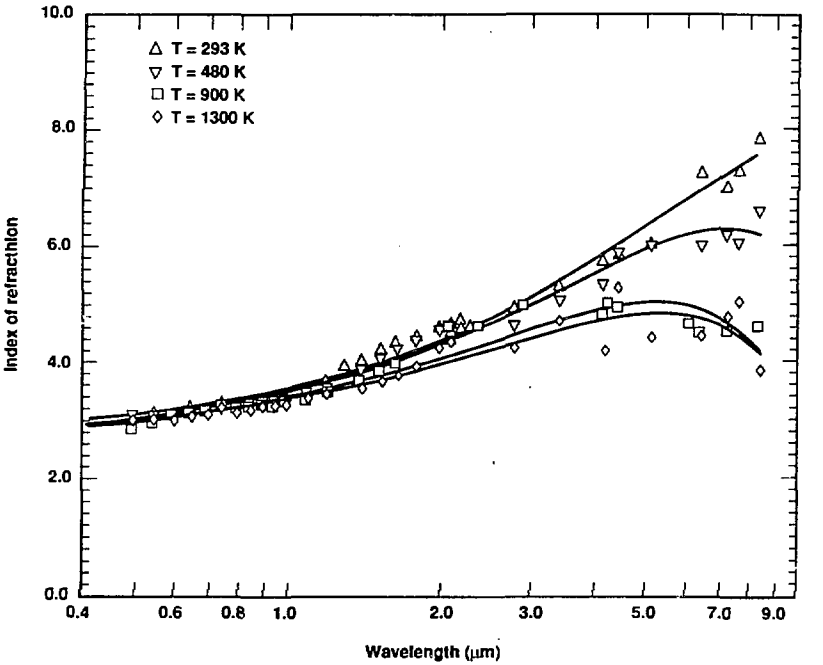

Fig. 5. The index of refraction of HOPG.

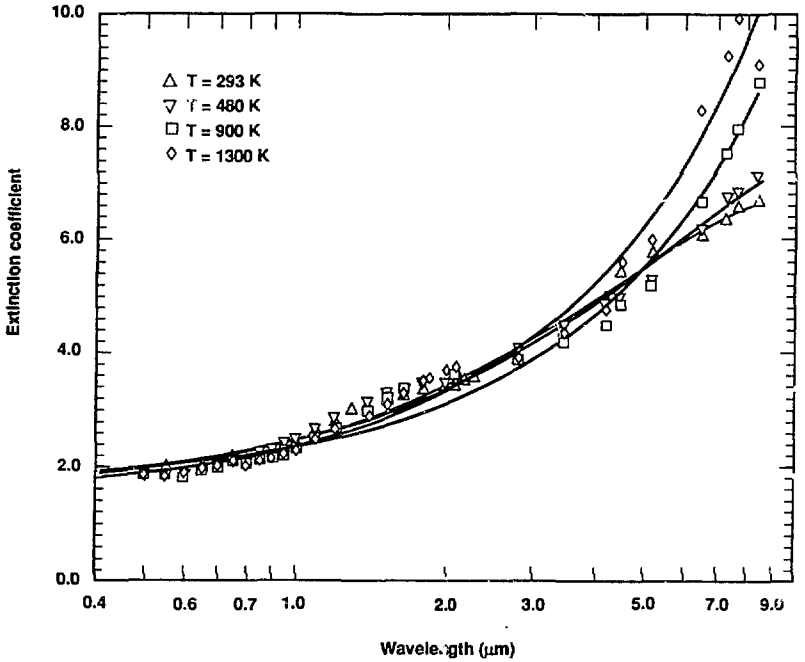

Figure. 6. The extinction coefficient of HOPG.

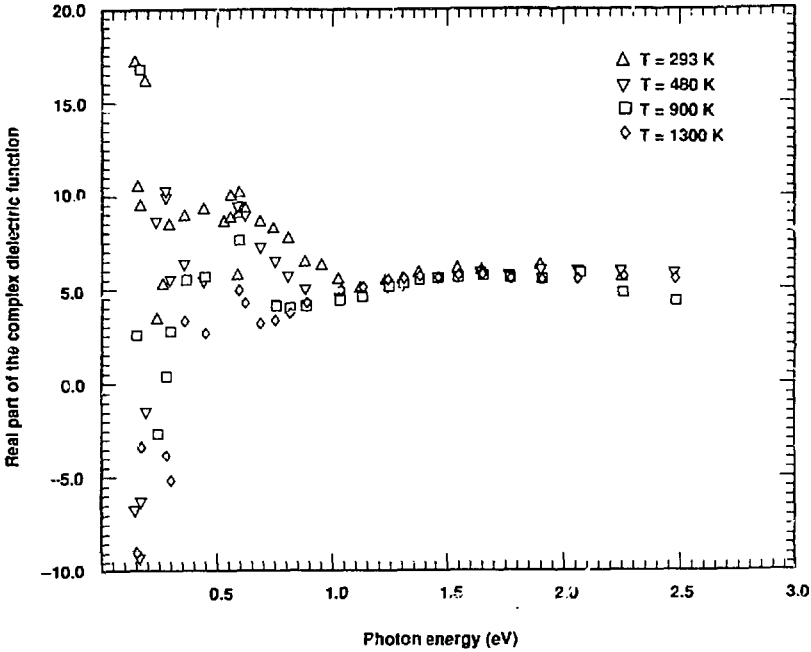

Fig. 7. The real part of the complex dielectric function of HOPG.

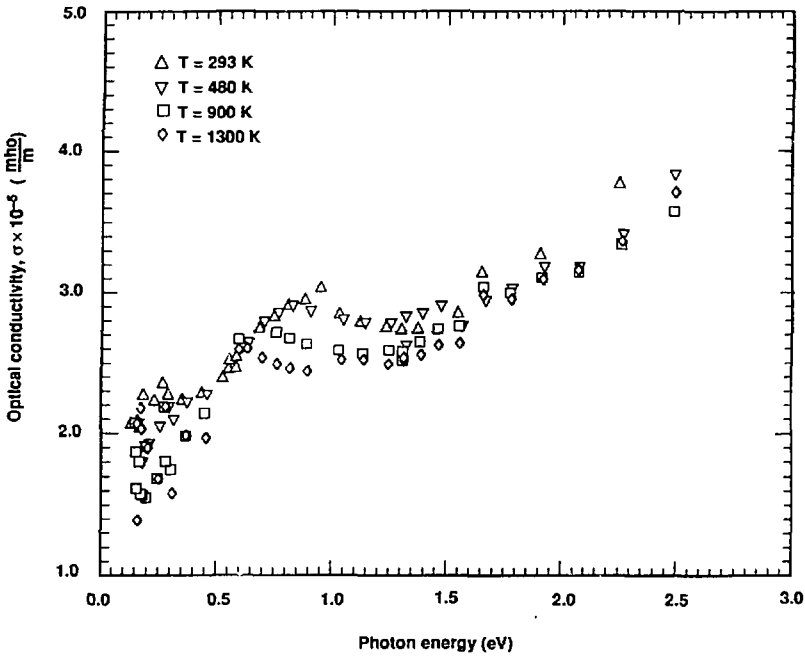

Fig. 8. The conductivity of HOPG.

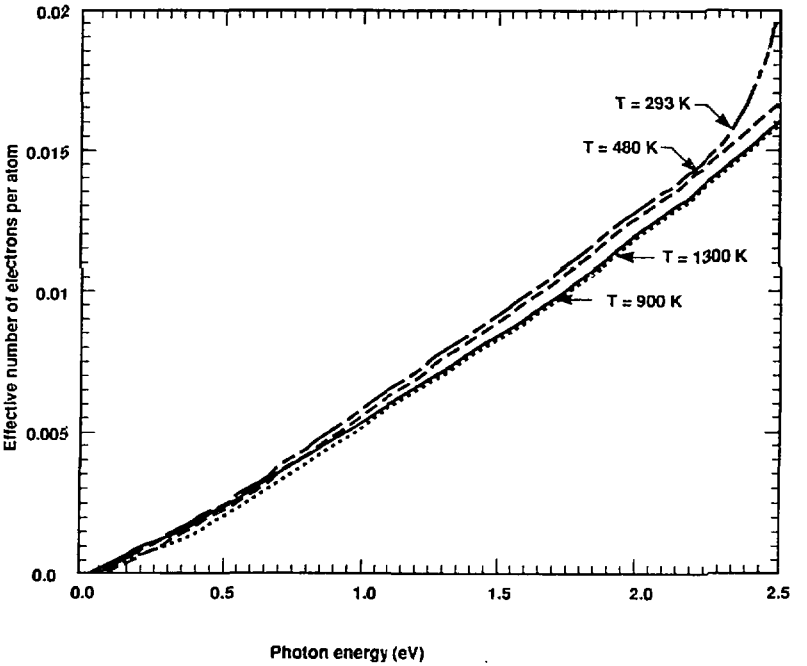

Fig. 9. The effective number of electrons per atom versus photon energy obtained from integration of curve fits to the results for conductivity.

Table 1

Coefficients for the curve fit to the normal spectral emissivity of HOPG as a function of wavelength.

Temperature = 293K

Coefficient	Value
a_0	1.589e-1
a_1	1.360e-4
a_2	1.033
a_3	1.654

Temperature = 480K

Coefficient	Value
a_0	1.667e-1
a_1	0.579e-4
a_2	1.144
a_3	1.580

Temperature = 900K

Coefficient	Value
a_0	-1.500e-2
a_1	0.319e-5
a_2	0.392
a_3	1.384

Temperature = 1300K

Coefficient	Value
a_0	-1.439e-1
a_1	1.057e-5
a_2	0.266
a_3	1.173

Wavelength must be given in μm. The curve fit is of the form:

$$\varepsilon_n(\lambda) = a_0 + \frac{1}{a_1\lambda^2 + a_2\lambda + a_3}$$